

Accepted Manuscript

Late Holocene sea-level evolution of Paros Island (Cyclades, Greece)

Anna Karkani, Niki Evelpidou, Matthieu Giaime, Nick Marriner, Christophe Morhange,
Giorgio Spada



PII: S1040-6182(18)31240-0

DOI: <https://doi.org/10.1016/j.quaint.2019.02.027>

Reference: JQI 7768

To appear in: *Quaternary International*

Received Date: 26 November 2018

Revised Date: 14 February 2019

Accepted Date: 18 February 2019

Please cite this article as: Karkani, A., Evelpidou, N., Giaime, M., Marriner, N., Morhange, C., Spada, G., Late Holocene sea-level evolution of Paros Island (Cyclades, Greece), *Quaternary International* (2019), doi: <https://doi.org/10.1016/j.quaint.2019.02.027>.

This is a PDF file of an unedited manuscript that has been accepted for publication. As a service to our customers we are providing this early version of the manuscript. The manuscript will undergo copyediting, typesetting, and review of the resulting proof before it is published in its final form. Please note that during the production process errors may be discovered which could affect the content, and all legal disclaimers that apply to the journal pertain.

1 **Late Holocene sea-level evolution of Paros Island (Cyclades, Greece)**

2

3 Karkani Anna^{1*}, Evelpidou Niki², Giaime Matthieu³, Marriner Nick⁴, Morhange

4 Christophe⁵, Spada Giorgio⁶

5

6 ¹ Faculty of Geology and Geoenvironment, National and Kapodistrian University of

7 Athens, Panepistimiopolis, Zografou, 15784 Athens, Greece, email:

8 ekarkani@geol.uoa.gr

9 ² Faculty of Geology and Geoenvironment, National and Kapodistrian University of

10 Athens, Panepistimiopolis, Zografou, 15784 Athens, Greece, email:

11 evelpidou@geol.uoa.gr

12 ³ University of Durham, Department of Geography, South Road, DH1 3LE, Durham,

13 UK, email: matthieu.giaime@gmail.com

14 ⁴ CNRS, Laboratoire Chrono-Environnement UMR6249, Université de Franche-

15 Comté, UFR ST, 16 Route de Gray, 25030 Besançon, France, email:

16 nick.marriner@univ-fcomte.fr

17 ⁵ Aix Marseille University, CNRS, IRD, Coll France, CEREGE, Aix-en-Provence,

18 France; RIMS, The Leon Recanati Institute for Maritime Studies University of Haifa,

19 31905, Israel , email: morhange@cerege.fr

20 ⁶ Dipartimento di Scienze Pure e Applicate (DiSPeA), Università di Urbino “Carlo

21 Bo”, Italy, email: giorgio.spada@gmail.com

22

23 * corresponding author

24

25 **Abstract**

26 Relative sea-level (RSL) reconstructions are essential to answer a variety of scientific
27 questions, ranging from the investigation of crustal movements to the calibration of
28 earth rheology models and ice sheet reconstructions.

29 It is generally assumed that most Cycladic islands (Aegean Sea, Greece) are affected
30 by a gradual subsidence, attributed to the crustal thinning and to hydro-isostatic
31 processes that accompanied the post-glacial rise in sea level. In this paper, we produce
32 new RSL data from sedimentary records on Paros Island. We compare and contrast
33 these RSL data with published data from the nearby island of Naxos. Our results are
34 further compared with sea-level predictions from two different GIA models in an
35 attempt to better quantify the tectonic regime of the wider study area. Our findings
36 suggest average tectonic subsidence rates close to 1.0 ± 0.4 mm/yr since 5500 cal BP.
37 These rates are not linear in time and have increased since 2500 cal BP.

38

39

40 Keywords: relative sea level, subsidence, coastal geomorphology, lagoon, Holocene,
41 central Aegean

42

43 **1. Introduction**

44 Sea-level changes are driven either by variations in the masses or volume of the
45 oceans, defined as ‘eustatic’, or by changes of the land with respect to the sea surface,
46 called ‘relative’ (Rovere *et al.*, 2016). During the past 4000 years, the ice-equivalent
47 melt-water input is considered minimal (Peltier, 2002; Milne *et al.*, 2005; Church *et*
48 *al.*, 2008). Therefore, any significant changes in relative sea-level (RSL) are almost
49 entirely driven by vertical land movements caused by tectonics and glacial isostatic
50 adjustment (GIA) or sediment compaction (Engelhart *et al.*, 2009).

51 RSL reconstructions are key to probing various research questions, ranging from the
52 calibration of earth rheology models and ice sheet reconstructions to the investigation
53 of crustal movements (Lambeck *et al.*, 2004; Peltier, 2004; Engelhart and Horton,
54 2012). GIA models have often been employed to identify stable and unstable areas
55 and deduce tectonic rates through comparisons with observational data (e.g. Sivan *et*
56 *al.*, 2001; 2004; Pirazzoli, 2005; Pavlopoulos *et al.*, 2011; Stiros *et al.*, 2011; Van De
57 Plassche *et al.*, 2014; Woodroffe *et al.*, 2015; Bradley *et al.*, 2016; Chelli *et al.*, 2017;
58 Vacchi *et al.*, 2017; Melis *et al.*, 2018). Greece, like the rest of the Mediterranean, is
59 characterized by small tidal ranges that favor the preservation of sea level indicators
60 (e.g. Rovere *et al.*, 2012).

61 In this context, the main aim of this study is to elucidate the relative sea-level history
62 of Paros island during the Late Holocene (i.e., last 4000 years), through the
63 multiproxy analysis of a sediment core from the western part of the island, in
64 combination with published data from the central Cyclades. We compare and contrast
65 our results with new modelled curves for Paros island, in an attempt to reconstruct
66 RSL changes and assess the tectonic regime of the central Cyclades.

67

68 **2. Regional Setting**

69 The Cycladic Plateau has been subjected to successive stages of emergence and
70 submergence due to changing sea level during the Quaternary (Kapsimalis *et al.*,
71 2009). The central Aegean is considered to be an area of low seismicity, characterized
72 by the absence of large earthquakes (Fig. 1) (e.g. Papazachos, 1990; Sakellariou and
73 Galanidou, 2016). According to Sakellariou and Galanidou (2016), vertical tectonic
74 movements are of minor significance and the coastal evolution of the central Aegean

75 during Late Pleistocene-Holocene is mostly affected by eustatic sea-level fluctuations
76 and, to a lesser degree, by isostatic movements.

77 Lykousis (2009) noted a continuous subsidence rate during the last 400 ka, with
78 values of 0.34–0.60 mm/yr for the Cycladic plateau, with a gradual decrease in the
79 magnitude of the extensional tectonic regime. According to Tirel *et al.* (2004), the
80 Cyclades probably act as a rigid block translated toward the south–west with no
81 significant deformation, in agreement with GPS velocities and a lack of major
82 earthquakes.

83 The Island of Paros lies in the central Aegean Sea, constituting the third largest island
84 in the Cyclades archipelago (Fig. 1, 2). Paros forms a NE–SW trending dome
85 bounded by a low-angle inactive normal fault to the east and northeast (Bargnesi *et*
86 *al.*, 2013). It has a rocky coastal zone, particularly in the northern part, characterized
87 by the alternation of carbonate rocks, gneisses-schists and alluvial deposits
88 (Papanikolaou, 1996). Beaches form a smaller part of coastal zone, mainly near
89 coastal plains in the eastern part of the island.

90 The coring site, Pounta (POU2) is located in the western coast of Paros (Fig. 2a).

91 POU2 core was drilled on the southwest coast, 1 km south of Pounta (Fig. 2a, b).

92 Today, the area is characterized by the presence of coastal dunes, forming a sandy
93 spit/barrier that frames a leeward lagoon.

94

95 **3. Materials and Methods**

96 **3.1 Palaeoenvironmental reconstruction**

97 A borehole was drilled with a portable drilling sampler, 35 mm in diameter, reaching
98 a maximum depth of 4 m below mean sea level (msl). For the palaeoenvironmental
99 reconstruction, multiproxy analyses were undertaken, which included

100 sedimentological analysis of the core, biostratigraphy of the macrofauna and
101 ostracods and radiocarbon dating.

102 The core was analyzed at Chrono-environment (CNRS, University of Franche-Comté,
103 Besançon, France). The core was first studied and photographed in detail in order to
104 record the general stratigraphy. The sediment texture was determined by separating
105 out the gravel (>2 mm), sand (2 mm to 50 μm) and silt/clay (<50 μm) fractions, using
106 two sieve mesh sizes, 2 mm and 50 μm .

107 The gravel fraction of the sediments was examined to identify mollusc shells and
108 determine their ecology. The identifications and classifications are based on d'
109 Angelo and Gargiullo (1978) and Doneddu and Trainito (2005). The species were
110 assigned to ecological groups defined by Pérès and Picard (1964) and Pérès (1982).
111 Ostracods were extracted from the dry sand fraction (>150 μm). The identified taxa
112 were assigned to assemblages based on their ecological preferences: freshwater,
113 lagoonal, marine lagoonal, coastal and marine (Lachenal, 1989; Nachite *et al.*, 2010;
114 Salel *et al.*, 2016).

115

116

117 **3.2 Chronology**

118 The chronostratigraphy of the core is based on four AMS radiocarbon dates
119 performed at the Poznan Radiocarbon Laboratory (Poland) (Table 1). The radiocarbon
120 ages of the samples were calibrated using the online software Calib 7.10 (Stuiver *et*
121 *al.*, 2016) with the Marine13 curve (Reimer *et al.*, 2013). Ages of the shell samples
122 were corrected for the local marine reservoir effect according to Reimer & McCormac
123 (2002), using a mean ΔR value of 154 ± 52 for the Aegean Sea.

124

125 **3.3 Sea-level reconstruction**

126 Results of the paleo-environmental reconstruction of the new core revealed facies
127 characteristic of coastal and lagoonal environments. We produced a new suite of RSL
128 index points following the protocol developed by Vacchi *et al.* (2016), which has
129 been used in a number of recent Mediterranean studies (e.g. Vacchi *et al.*, 2017, 2018;
130 Karkani *et al.*, 2017; Fontana *et al.*, 2017; Melis *et al.*, 2017, 2018). The indicative
131 meaning of each index point is composed of a reference water level (RWL) and the
132 indicative range (IR). The IR corresponds to the elevation interval over which an
133 indicator is formed and the RWL is the midpoint of this range, expressed relative to
134 the same datum as the elevation of the sampled indicator (e.g. Horton and Shennan,
135 2009; Gehrels and Woodworth, 2013; Hijma *et al.*, 2015).

136 For the production of RSL index points from the core, we attributed an indicative
137 range from 0 to -2 m for samples found in an open or marine-influenced lagoon and
138 an indicative range from 0 to -1 m for an inner or semi-enclosed lagoon (Vacchi *et al.*,
139 2016). Although no modern analogues have been reported in the literature for the
140 study area, the indicative ranges reported by Vacchi *et al.* (2016) have been adopted
141 considering the geomorphological status of the coastal lagoons in the Cyclades. More
142 precisely, in the Cycladic area, and on Paros in particular, the contemporary coastal
143 lagoons are usually dry during the summer while, during winter, their depths do not
144 exceed 1-2 m. We added additional vertical errors to each index point, including: a)
145 an error of ± 0.2 m for the samples altitude and b) a core stretching/shortening error of
146 0.15m (Hijma *et al.*, 2015).

147 RSL index points were further produced using samples deposited in semi-enclosed
148 lagoon facies from Evelpidou *et al.* (2012) and from Karkani *et al.* (2018), and from
149 samples found in a brackish environment, most likely deposited within ± 0.5 m of

150 former MSL (Pavlopoulos *et al.*, 2011; Evelpidou *et al.*, 2012; Karkani *et al.*, 2017)
151 (Fig. 2a). We further took into consideration the beachrock luminescence dating
152 results from Karkani *et al.* (2017) for Paros and Naxos (Fig. 2a). Various studies in
153 the eastern Mediterranean have shown that beachrocks are accurate sea-level
154 indicators, as long as they are supported by cement mineralogy and morphology and,
155 if possible, by sedimentary information (e.g. Desruelles *et al.*, 2009; Mauz *et al.*,
156 2015). The dated beachrock samples of the study area showed clear intertidal
157 formation based on cement characteristics and therefore an indicative range between
158 the Mean High Tide (MHT) and Mean Low Tide (MLT) (i.e. 0.14 m; HNHS, 2012)
159 was considered (Karkani *et al.*, 2017).

160 To interpret the observational RSL data, we considered predictions from two Glacial
161 Isostatic Adjustment (GIA) models. The first is ICE-6G (VM5a) of Peltier *et al.*
162 (2015) while the second (ANU), is the latest version of the GIA model progressively
163 developed by K. Lambeck and co-workers (see Lambeck *et al.* 2003 and further
164 refinements). For both GIA models, we solved the Sea Level Equation using an
165 improved version of the program SELEN (Spada and Stocchi, 2007), in which the
166 horizontal migration of shorelines, the transition between grounded and floating ice
167 and the rotational feedback on sea-level are taken into account. The two GIA models
168 are characterized by different chronologies for the melting of the late-Pleistocene ice
169 sheets but also different rheological profiles. In particular, while in ICE-6G (VM5a)
170 the lower mantle viscosity is $3.2 \cdot 10^{21}$ Pa.s, for ANU we adopted a value 10^{22} Pa.s,
171 in the range suggested in the study of Lambeck *et al.* (2017). The relatively high
172 lower mantle viscosity in ANU compared to ICE-6G (VM5a) generally implies a
173 larger isostatic disequilibrium and higher rates of glacial-isostatic readjustment during
174 the last few millennia, consistent with the results below.

175

176 **4. Results**177 **4.1 Lithology-faunal evidence - depositional environment**178 Unit A: shallow marine environment

179 Unit A, from the bottom of the core (4 m) up to 2.6 m b.s.l. is dominated by medium
180 to coarse sand with shell fragments (Fig. 3, 4). The sand fraction comprises more than
181 87% of the total sediment texture. The macrofauna (Fig. 3) is dominated by
182 infralittoral sand assemblages (e.g. *Truncatella subcylindrica*, *Rissoa lineolata*, *Rissoa*
183 *monodonta*, *Tricolia pullus*), hard substrate assemblages (e.g. *Conus mediterraneus*,
184 *Gibbula spp.*, *Jujubinus sp.*, *Gibbula varia*, *Cythara paciniana*) and species living on
185 algae. Ostracods are almost absent with the exception of a few coastal (45.7%)
186 (*Aurila convexa*, *Aurila woodwardii*, *Cytherelloidea sordida*, *Hiltermannicythere cf.*,
187 *Urocythereis oblonga*, *Cytherois frequens*, *Neocytherideis fasciata*, *Costa edwardsii*)
188 and marine lagoonal species (54.3%) (*Loxoconcha stellifera*, *Xestoleberis communis*,
189 *Xestoleberis sp.*) at ~3.3 m depth (Fig. 4). This unit represents a shallow marine
190 environment. Two marine shells were dated from the middle and the top of this unit
191 (*Nassarius lousi* and *Cerithium vulgatum*, respectively; see Table 1), however, the
192 deeper sample (490±30 BP) yielded an age younger than the other shallower samples.
193 The top of the unit was dated to 964-1229 cal AD (721-986 cal BP).

194

195 Unit B: Leaky coastal lagoon

196 Unit B is found between 2.46 m and 1.18 m b.s.l., consisting of silty sand with
197 *Posidonia oceanica* fibers and shell fragments. The unit presents a finer sedimentation
198 towards the top. Gravels comprise 2.1% of the total sediment texture, sands 71.6%
199 and silts-clays 26.3%. The macrofauna is dominated by lagoonal (*Loripes lacteus*,

200 *Abra segmentum*), upper muddy sand assemblages in sheltered areas (*Acanthocardia*
201 *echinata*, *Cerithium vulgatum*), and infralittoral sand assemblages (*Tricolia pullus*,
202 *Tricolia tenuis*, *Rissoa lineolata*, *Rissoa guerini*, *Mitra ebenus*). Microfossil
203 assemblages are dominated by marine lagoonal (72.4%) (*Loxoconcha stellifera*,
204 *Xestoleberis communis*) and coastal species (26%) (*Cytherelloidea sordida*). The
205 middle of this unit was dated to 1652-1910 cal AD (40-298 cal BP). This unit is
206 probably indicative of a leaky coastal lagoon, in constant connection with the sea
207 (Kjerfve, 1994).

208

209 Unit C: Lagoon periodically connected with the sea

210 Unit C is found from 1.18 m b.s.l. until the top of the core and consists of coarse to
211 medium sand, which becomes siltier towards the top. The sands fraction represents
212 91% of the total sediment texture up to 50 cm depth and the proportion of silts-clays
213 increases in the last 50 cm reaching 25.4%. Macrofauna analysis indicates that
214 assemblages are poorer in terms of abundance and mainly consist of upper muddy
215 sand assemblages in sheltered areas (*Cerithium vulgatum*), upper-clean sand
216 assemblages (e.g. *Conus mediterraneus*, *Cardita calyculata*, *Gibbula spp.*), hard
217 substrate species and algae. Ostracods are dominated by marine lagoonal species
218 (75.6%) (e.g. *Loxoconcha stellifera*, *Xestoleberis communis*, *Loxoconcha*
219 *rhomboidea*); lagoonal species are represented by few individuals of *Cyprideis torosa*
220 (3.5%), and coastal species (18.4%) (e.g. *Aurila convexa*, *Cytherelloidea sordida*,
221 *Urocythereis oblonga*, *Cytherois frequens*). This unit is probably indicative of a
222 lagoon more periodically connected with the sea (“choked lagoon” according to the
223 classification of Kjerfve (1994). The middle of this unit was dated to 520±30 BP.

224

225

226 **5. Discussion**

227 Most Cycladic islands are generally considered to be affected by a gradual
228 subsidence, which is attributed to the crustal thinning, in an extensional tectonic
229 regime (e.g. Mercier *et al.*, 1989; Sakellariou & Tsampouraki-Kraounaki, 2019). The
230 absence of morphological features indicative of uplift in the coastal zone, such as
231 marine terraces or benches, elevated beachrocks, marine notches, or raised Quaternary
232 coastal deposits are taken to substantiate this absence of local uplift. A subsidence
233 regime has been noted by several authors for the wider study area (e.g. Desruelles *et*
234 *al.*, 2009; Lykousis, 2009; Evelpidou *et al.*, 2012; 2014; Karkani *et al.*, 2017).

235 The reconstructed RSL history from Paros and Naxos Islands is shown in Fig. 5. We
236 included RSL estimates derived from archaeological data. In particular, according to
237 Morrison (1968), a RSL rise of 5.5 m since 5500 BP may be estimated for Antiparos
238 island, based on the Neolithic settlement of Saliagos. A RSL between -2 and -3 m
239 around 2500–2900 BP has been estimated by Papathanassopoulos and Schilardi
240 (1981), based on a number of archaeological findings around Paros Island (e.g.
241 submerged moles, graves, buildings) (Fig. 5).

242 Overall, our new data support a RSL that rose by ~2 m in the last 2000 years, and by
243 at least ~3.9 m since ~4500 years BP (Fig. 5). Conversely, two brackish samples from
244 a core in Mikri Vigla (Naxos Island, Evelpidou *et al.*, 2012), indicate that RSL
245 reached ~-2 m \pm 0.5 at about ~4.0 ka. Similarly, two lagoonal samples from the Livadia
246 core (Paros Island, Karkani *et al.* 2018) suggest a sea level between -1.5 and -2.5 m
247 around 3100-3300 years BP. In both cases (Mikri Vigla and Livadia), the samples
248 were rejected as they provided ages inconsistent with the chronostratigraphy.

249 In comparison with the modelled curves, which account for the effect of GIA, for
250 Paros Island (Fig. 5), our RSL points have a lower position. To evaluate the tectonic
251 component, we subtracted the elevation of the produced index points, from that of the
252 corresponding points inferred from the GIA models at the same age (e.g. Chelli *et al.*,
253 2017). Average rates of tectonic subsidence were calculated for three different time
254 frames (present to ~5500 cal BP, present day to 2500 cal BP, 2500 cal BP to 5500 cal
255 BP), based on the mismatch between models and observations for Paros and the wider
256 study area, considering the difference in elevation between sea level estimates from
257 our data and from each of the models employed.

258 Since ~5500 cal BP, comparable tectonic subsidence rates ($\sim 1.0 \pm 0.4$ mm/yr) are
259 found when the RSL data are corrected for the predictions of the two GIA models.

260 The average rate of tectonic subsidence appears lower for the timespan 2500-5000 cal
261 BP, being close to 0.7 ± 0.2 mm/yr, and higher ($\sim 1.2 \pm 0.4$ mm/yr) since 2500 cal BP. It
262 appears evident from our findings that subsidence rates in the central Cyclades (Paros
263 and Naxos) have not been constant since ~5500 cal BP. This suggests that, since
264 ~2500 cal BP, the study area has been affected by seismic events that produced
265 vertical displacements and/or during this time span the subsidence rate increased.

266 Evidence of seismic events, since about 3300 BP, have been reported in the study area
267 by Evelpidou *et al.* (2014) through the analysis of submerged tidal notches,
268 suggesting that at least part of the observed subsidence is related to vertical seismic
269 displacements. Evelpidou *et al.* (2014) identified former shorelines at depths between
270 280 ± 20 and 30 ± 5 cm below modern sea level. In a recent study Vamvakaris *et al.*
271 (2016), calculated the mean return period values for shallow earthquakes with $M > 6.0$
272 in the Aegean region and suggested very long return periods (> 200 years) for the
273 broader Cyclades plateau, amongst other areas. The same authors also found that the

274 most probable maximum magnitudes for a return period of 50 yr is expected to be less
275 than $M=5.0$, for low seismicity areas, such as the Cyclades islands plateau. In the
276 Cyclades, one of the largest earthquakes in the last century occurred in July 1956,
277 southwest of Amorgos Island, with a magnitude of 7.4, which was followed (a few
278 minutes later) by a second of M_s 7.2 (e.g. Stiros et al., 1994; Okal *et al.*, 2009; Brüstle
279 *et al.*, 2014).

280 For decades the Cycladic plateau has been considered as a tectonically inactive area
281 (Sakellariou and Tsampouraki-Kraounaki, 2019). Our findings suggest that tectonic
282 subsidence has contributed to the late Holocene evolution of the central Cyclades and
283 it is most likely owed to a combination of seismic events and gradual long-term
284 subsidence, due to the dominance of an extensional structural pattern. Furthermore,
285 subsidence rates are higher than previously calculated for the study area (e.g.
286 Pavlopoulos *et al.*, 2011).

287

288 **6. Conclusions**

289 Our study focused on the reconstruction of RSL changes in the central Cyclades
290 through the analysis of new and published sea-level data. We reevaluated the tectonic
291 regime of the central Cyclades through the comparison of our data with new modelled
292 RSL curves for Paros Island. Our findings suggest average tectonic subsidence rates
293 close to 1 mm/yr since 5500 cal BP, which do not appear constant during the late
294 Holocene; these values have increased since 2500 cal BP. The subsidence trend in the
295 central Cyclades is most likely a combination of seismic events and gradual long-term
296 subsidence, due to the dominance of an extensional structural pattern.

297

298

299 Acknowledgements

300 The authors would like to thank Alexandros Petropoulos, Giannis Saitis, Theophilos
301 Valsamidis, Matina Seferli and Electra Kotopoulou for their help during fieldwork in
302 Paros.

303 This work was co-funded by the General Secretariat for Research and Technology
304 (GSRT) and the European Regional Development Fund, in the framework of the
305 Bilateral project Greece – France entitled: ‘Sea level changes in Cyclades’.

306 This work has been partially carried out thanks to the support of the Labex OT-Med
307 (ANR-11-LABX-0061) and of the A*MIDEX project (n° ANR-11-IDEX-0001-02),
308 funded by the « Investissements d’Avenir » French Government program, managed by
309 the French National Research Agency (ANR).

310 GS is funded by a FFABR (Finanziamento delle Attività Base di Ricerca) grant of the
311 MIUR (Ministero dell’Istruzione, dell’Università e della Ricerca) and by a DiSPeA
312 research grant.

313

314 Figure captions

315 Fig. 1. Location of the study area and seismicity since 550 B.C. (seismicity data
316 retrieved from http://geophysics.geo.auth.gr/ss/station_index_en.html). The red square
317 denotes the location of Paros Island. The bathymetry was provided by EMODnet
318 Bathymetry 2015.

319 Fig. 2: a) Location of the drilling site on Paros Island and sea-level data used in this
320 study from Evelpidou *et al.* (2012) and Karkani *et al.* (2017; 2018), b) Aerial view of
321 Pounta coring site.

322 Fig. 3. Core POU2 stratigraphy and macrofauna.

323 Fig. 4. Core POU2 stratigraphy and ostracods.

324 Fig. 5: Late Holocene RSL data from this study, compared with beachrock data from
325 Karkani *et al.* (2017) and sediment corings from Paros (Karkani *et al.*, 2018) and
326 Naxos (Evelpidou *et al.*, 2012). The circled samples are in disagreement with the rest
327 of RSL index points. The RSL curves for Paros Island were obtained by numerically
328 solving the Sea-Level Equation. The GIA models ICE-6G (solid) and ANU (dashed)
329 have been employed.

330

331 **Table captions**

332 Table 1. Radiocarbon ages for dated samples from the Paros core. The data were
333 calibrated using the online software Calib 7.10 (Stuiver *et al.*, 2016) with the
334 Marine13 curve (Reimer *et al.*, 2013). Shell samples were corrected for the local
335 marine reservoir effect according to Reimer & McCormac (2002), using a mean ΔR
336 value of 154 ± 52 for the Aegean Sea.

337

338 **References**

- 339 Bargnesi, E.A., Stockli, D.F., Mancktelow, N., Soukis, K., 2013. Miocene core
340 complex development and coeval supradetachment basin evolution of Paros,
341 Greece, insights from (U–Th)/He thermochronometry. *Tectonophysics* 595–596,
342 165–182. doi:10.1016/j.tecto.2012.07.015
- 343 Bradley, S. L., Milne, G. A., Horton, B. P., Zong, Y., 2016. Modelling sea level data
344 from China and Malay-Thailand to estimate Holocene ice-volume equivalent sea
345 level change. *Quaternary Science Reviews* 137, 54–68.
346 <https://doi.org/10.1016/J.QUASCIREV.2016.02.002>
- 347 Brüstle, A., Friederich, W., Meier, T., Gross, C., 2014. Focal mechanism and depth of
348 the 1956 Amorgos twin earthquakes from waveform matching of analogue

- 349 seismograms. *Solid Earth* 5, 1027-1044, <https://doi.org/10.5194/se-5-1027-2014>,
350 2014.
- 351 Chelli, A., Pappalardo, M., Bini, M., Brückner, H., Neri, G., Neri, M., Spada, G.,
352 2017. Assessing tectonic subsidence from estimates of Holocene relative sea-level
353 change: An example from the NW Mediterranean (Magra Plain, Italy). *The*
354 *Holocene* 27(12), 1988–1999. <https://doi.org/10.1177/0959683617715688>
- 355 Church, J.A., White, N.J., Aarup, T., Wilson, W.S., Woodworth, P.L., Domingues,
356 C.M., Hunter, J.R., Lambeck, K., 2008. Understanding global sea levels: past,
357 present and future. *Sustain. Sci.* 3, 9-22.
- 358 d'Angelo, G., Gargiullo, S., 1978. *Guida alle conchiglie Mediterranee*. Fabbri Editori,
359 Milano.
- 360 Desruelles, S., Fouache, É., Ciner, A., Dalongeville, R., Pavlopoulos, K., Kosun, E.,
361 Coquinot, Y., Potdevin, J.-L., 2009. Beachrocks and sea level changes since
362 Middle Holocene: Comparison between the insular group of Mykonos–Delos–
363 Rhenia (Cyclades, Greece) and the southern coast of Turkey. *Global and Planetary*
364 *Change* 66, 19–33. doi:10.1016/j.gloplacha.2008.07.009
- 365 Doneddu, M., Trainito, E., 2005. *Conchiglie del Mediterraneo*. Il Castello, Trezzano
366 sul Naviglio.
- 367 Engelhart, S.E., Horton, B.P., 2012. Holocene sea level database for the Atlantic coast
368 of the United States. *Quaternary Science Reviews* 54, 12-25.
- 369 Engelhart, S.E., Horton, B.P., Douglas, B.C., Peltier, W.R., Horton, B.P., Tornqvist,
370 T.E., 2009. Spatial variability of late Holocene and 20th century sea-level rise
371 along the Atlantic coast of the United States. *Geology* 37, 1115-1118.

- 372 Evelpidou, N., Pavlopoulos, K., Vassilopoulos, A., Triantafyllou, M., Vouvalidis, K.,
373 Syrides, G., 2012. Holocene palaeogeographical reconstruction of the western part
374 of Naxos island (Greece). *Quaternary International* 266, 81-93.
- 375 Evelpidou, N., Melini, D., Pirazzoli, P., Vassilopoulos, A., 2014. Evidence of
376 repeated Late Holocene subsidence in the SE Cyclades (Greece) deduced from
377 submerged notches. *International Journal of Earth Sciences* 103 (1), 381-395. doi:
378 10.1007/s00531-013-0942-0.
- 379 Fontana, A., Vinci, G., Tasca, G., Mozzi, P., Vacchi, M., Bivi, G., Salvador, S.,
380 Rossato, S., Antonioli, F., Asioli, A., Bresolin, M., Di Mario, F., Hajdas, I., 2017.
381 Lagoonal settlements and relative sea level during Bronze Age in Northern
382 Adriatic: Geoarchaeological evidence and paleogeographic constraints. *Quaternary*
383 *International* 439, 17–36. <https://doi.org/10.1016/j.quaint.2016.12.038>
- 384 Gehrels, W.R., Woodworth, P.L., 2013. When did modern rates of sea-level rise start?
385 *Global and Planetary Change* 100, 263-277. DOI: 10.1016/j.gloplacha.2012.10.020
- 386 Hellenic Navy Hydrographic Service (HNHS), 2012. Statistical data for sea level of
387 the Greek ports. HNHS, Athens (in Greek).
- 388 Hijma, M.P., Engelhart, S.E., Törnqvist, T.E., Horton, B.P., Hu, P., Hill, D.F., 2015.
389 A protocol for a geological sea-level database. In: Shennan, I., Long, A., Horton,
390 B.P. (Eds.), *Handbook of Sea-Level Research*. Willey, pp. 536–553.
391 doi:10.1002/9781118452547.ch34
- 392 Horton, B.P., Shennan, I., 2009. Compaction of Holocene strata and the implications
393 for relative sea level change on the east coast of England. *Geology* 37, 1083-1086.
- 394 Kapsimalis, V., Pavlopoulos, K., Panagiotopoulos, I., Drakopoulou, P., Vandarakis,
395 D., Sakelariou, D., Anagnostou, C., 2009. Geoarchaeological Challenges in the

- 396 Cyclades Continental Shelf (Aegean Sea). *Zeitschrift für Geomorphologie* 53
397 (Suppl. 1), 169-190.
- 398 Karkani, A., Evelpidou, N., Vacchi, M., Morhange, C., Tsukamoto, S., Frechen, M.,
399 Maroukian, H., 2017. Tracking shoreline evolution in central Cyclades (Greece)
400 using beachrocks. *Marine Geology* 388, 25–37.
401 <https://doi.org/10.1016/j.margeo.2017.04.009>
- 402 Karkani, A., Evelpidou, N., Giaime, M., Marriner, N., Maroukian, H., Morhange, C.,
403 2018. Late Holocene palaeogeographical evolution of Paroikia Bay (Paros Island,
404 Greece). *Comptes Rendus Geoscience* 350 (5), 202-211.
405 <https://doi.org/10.1016/j.crte.2018.04.004>
- 406 Kjerfve, B., 1994. Coastal Lagoons. In: Kjerfve, B. (Ed.), *Coastal Lagoon Processes*.
407 Elsevier, pp. 1-8. <https://doi.org/doi:10.1201/EBK1420088304-c1>
- 408 Lachenal, A.M., 1989. *Écologie des ostracodes du domaine méditerranéen:*
409 *application au Golfe de Gabès (Tunisie orientale). Les variations du niveau marin*
410 *depuis 30 000 ans. Documents des laboratoires de géologie de Lyon* 108, 1–239.
- 411 Lambeck, K., Purcell, A., Johnston, P., Nakada, M., Yokoyama, Y., 2003. Water-load
412 definition in the glacio-hydro-isostatic sea-level equation. *Quaternary Science*
413 *Reviews* 22(2), 309-318.
- 414 Lambeck, K., Antonioli, F., Purcell, A., Silenzi, S., 2004. Sea-level change along the
415 Italian coast for the past 10,000 yr. *Quaternary Science Reviews* 23, 1567-1598.
- 416 Lykousis, V., 2009. Sea-level changes and shelf break prograding sequences during
417 the last 400ka in the Aegean margins: Subsidence rates and palaeogeographic
418 implications. *Continental Shelf Research* 29, 2037–2044.
419 [doi:10.1016/j.csr.2008.11.005](https://doi.org/10.1016/j.csr.2008.11.005)

- 420 Mauz, B., Vacchi, M., Green, A., Hoffmann, G., Cooper, A., 2015. Beachrock: A tool
421 for reconstructing relative sea level in the far-field. *Marine Geology* 362, 1–16.
422 <https://doi.org/10.1016/j.margeo.2015.01.009>
- 423 Melis, R.T., Depalmas, A., Di Rita, F., Montis, F., Vacchi, M., 2017. Mid to late
424 Holocene environmental changes along the coast of western Sardinia
425 (Mediterranean Sea). *Global and Planetary Change* 155, 29–41.
426 <https://doi.org/10.1016/J.GLOPLACHA.2017.06.001>
- 427 Melis, R. T., Di Rita, F., French, C., Marriner, N., Montis, F., Serreli, G., Sulas, F.,
428 Vacchi, M., 2018. 8000 years of coastal changes on a western Mediterranean
429 island: A multiproxy approach from the Posada plain of Sardinia. *Marine Geology*
430 403, 93–108. <https://doi.org/10.1016/j.margeo.2018.05.004>
- 431 Mercier, J.-L., Sorel, D., Vergely, P., Simeakis, K., 1989. Extensional tectonic
432 regimes in the Aegean basins during the Cenozoic. *Basin Research* 2, 49–71
- 433 Milne, G.A., Long, A.J., Bassett, S.E., 2005. Modelling Holocene relative sea-level
434 observations from the Caribbean and South America. *Quaternary Science Reviews*
435 24, 1183-1202.
- 436 Morrison, I.A., 1968. Appendix I. Relative sea-level change in the Saliagos area since
437 Neolithic times. In: Evans, J.D., Renfrew, C. (Eds.), *Excavations at Saliagos Near*
438 *Antiparos*. Thames and Hudson, London, pp. 92-98.
- 439 Nachite, D., Rodríguez-Lázaro, J., Martín-Rubio, M., Pascual, A., Bekkali, R., 2010.
440 Distribution and ecology of recent ostracods from the Tahadart estuary (NW
441 Morocco). *Revue de Micropaleontologie* 53, 3–15.
- 442 Okal, E., Synolakis, C., Uslu, B., Kalligeris, N., Voukouvalas, E., 2009. The 1956
443 earthquake and tsunami in Amorgos, Greece. *Geophysical Journal International*
444 178, 1533–1554.

- 445 Papanikolaou, D., 1996. Geological map of Paros, scale 1:50000. IGME, Athens (in
446 Greek).
- 447 Papathanassopoulos, G., Schilardi, D., 1981. An underwater survey of Paros, Greece:
448 1979. Preliminary report. *The International Journal of Nautical Archaeology and*
449 *Underwater Exploration* 10 (2), 133-144.
- 450 Papazachos, B.C., 1990. Seismicity of the Aegean and surrounding area.
451 *Tectonophysics* 178, 287–308. doi:10.1016/0040-1951(90)90155-2
- 452 Pavlopoulos, K., Kapsimalis, V., Theodorakopoulou, K., Panagiotopoulos, I.P., 2011.
453 Vertical displacement trends in the Aegean coastal zone (NE Mediterranean)
454 during the Holocene assessed by geo-archaeological data. *The Holocene* 22 (6),
455 717-728.
- 456 Peltier, W.R., 2002. On eustatic sea level history: Last Glacial Maximum to
457 Holocene. *Quat. Sci. Rev.* 21, 377-396.
- 458 Peltier, W.R., 2004. Global glacial isostasy and the surface of the ice-age earth: the
459 ice-5G (VM2) model and grace. *Annual Review of Earth and Planetary Sciences*
460 32, 111-149.
- 461 Peltier, W.R., Argus, D.F., Drummond, R., 2015. Space geodesy constrains ice age
462 terminal deglaciation: the global ICE-6G-C (VM5a) model. *Journal of Geophysical*
463 *Research B: Solid Earth* 120(1), 450–487. doi: 10.1002/2014JB011176.
- 464 Pérès, J.-M., 1982. Major benthic assemblages. In: Kinne, O. (Ed.), *Marine Ecology*.
465 Wiley, Chichester, pp. 373–522.
- 466 Pérès, J.-M., Picard, J., 1964. *Nouveau manuel de bionomie benthique de la mer*
467 *Méditerranée*. Periplus, Marseille, 137 p.
- 468 Pirazzoli, P.A., 2005. A review of possible eustatic, isostatic and tectonic
469 contributions in eight late-Holocene relative sea-level histories from the

- 470 Mediterranean area. *Quaternary Science Reviews* 24 (18-19), 1989-2001.
471 <https://doi.org/10.1016/j.quascirev.2004.06.026>
- 472 Reimer, P.J., McCormac, F.G., 2002. Marine radiocarbon reservoir corrections for the
473 Mediterranean and Aegean Seas. *Radiocarbon* 44, 159-166.
- 474 Reimer, P.J., Bard, E., Bayliss, A., Beck, J.W., Blackwell, P.G., Bronk Ramsey, C.,
475 Buck, C.E., Cheng, H., Edwards, R.L., Friedrich, M., Grootes, P.M., Guilderson,
476 T.P., Haflidason, H., Hajdas, I., Hatté, C., Heaton, T.J., Hoffmann, D.L., Hogg,
477 A.G., Hughen, K.A., Kaiser, K.F., Kromer, B., Manning, S.W., Niu, M., Reimer,
478 R.W., Richards, D.A., Scott, E.M., Southon, J.R., Staff, R.A., Turney, C.S.M., van
479 der Plicht, J., 2013. IntCal13 and Marine13 radiocarbon age calibration curves 0–
480 50,000 years cal BP. *Radiocarbon* 55(4), 1869–1887.
- 481 Rovere, A., Stocchi, P., Vacchi, M., 2016. Eustatic and Relative Sea Level Changes.
482 *Current Climate Change Reports* 2, 221–231. doi:10.1007/s40641-016-0045-7
- 483 Rovere, A., Furlani, S., Benjamin, J., Fontana, A., Antonioli, F., 2012. MEDFLOOD
484 project: MEDiterranean sea-level change and projection for future FLOODing.
485 *Alpine and Mediterranean Quaternary* 25, 3–5.
- 486 Sakellariou, D., Galanidou, N., 2016. Pleistocene submerged landscapes and
487 Palaeolithic archaeology in the tectonically active Aegean region. *Geological*
488 *Society of London, Special Publication* 411, 145–178. doi:10.1144/SP411.9
- 489 Sakellariou, D., Tsampouraki-Kraounaki, K., 2019. Plio-Quaternary Extension and
490 Strike-Slip Tectonics in the Aegean. In: Duarte, J. (Ed.), *Transform Plate*
491 *Boundaries and Fracture Zones*. Elsevier, pp. 339–374.
492 <https://doi.org/10.1016/B978-0-12-812064-4.00014-1>

- 493 Salel, T., Bruneton, H., Lefèvre, D., 2016. Ostracods and environmental variability in
494 lagoons and deltas along the north-western Mediterranean coast (Gulf of Lions,
495 France and Ebro delta, Spain). *Revue de Micropaléontologie* 59 (4) 425-444.
- 496 Sivan, D., Wdowinski, S., Lambeck, K., Galili, E., Raban, A., 2001. Holocene sea-
497 level changes along the Mediterranean coast of Israel, based on archaeological
498 observations and numerical model. *Palaeogeography, Palaeoclimatology,*
499 *Palaeoecology* 167(1–2), 101–117. [https://doi.org/10.1016/S0031-0182\(00\)00234-](https://doi.org/10.1016/S0031-0182(00)00234-0)
500 [0](https://doi.org/10.1016/S0031-0182(00)00234-0)
- 501 Sivan, D., Lambeck, K., Toueg, R., Raban, A., Porath, Y., Shirman, B., 2004. Ancient
502 coastal wells of Caesarea Maritima, Israel, an indicator for relative sea level
503 changes during the last 2000 years. *Earth and Planetary Science Letters* 222, 315-
504 330. <https://doi.org/10.1016/j.epsl.2004.02.007>
- 505 Spada G, Stocchi P (2007) SELEN: a Fortran 90 program for solving the “Sea level
506 equation”. *Computers & Geosciences* 33(4), 538-562.
- 507 Stiros, S.C., Marangou, L., Arnold, M., 1994. Quaternary uplift and tilting of
508 Amorgos Island (southern Aegean) and the 1956 earthquake. *Earth and Planetary*
509 *Science Letters* 128(3-4), 65-76.
- 510 Stiros, S.C., Laborel, J., Laborel-Deguen, F., Morhange, C., 2011. Quaternary and
511 Holocene coastal uplift in Ikaria Island, Aegean Sea. *Geodinamica Acta* 24 (3-4),
512 123-131. doi:10.3166/ga.24.123-13
- 513 Stuiver, M., Reimer, P.J., and Reimer, R.W., 2016. CALIB 7.1 [WWW program] at
514 <http://calib.org>, accessed 2016-12-4.
- 515 Tirel, C., Gueydan, F., Tiberi, C., Brun, J.P., 2004. Aegean crustal thickness inferred
516 from gravity inversion. Geodynamical implications. *Earth and Planetary Science*
517 *Letters* 228, 267–280. doi:10.1016/j.epsl.2004.10.023

- 518 Vacchi, M., Marriner, N., Morhange, C., Spada, G., Fontana, A., Rovere, A., 2016.
519 Multiproxy assessment of Holocene relative sea-level changes in the western
520 Mediterranean: Sea-level variability and improvements in the definition of the
521 isostatic signal. *Earth-Science Reviews* 155, 172–197.
522 <https://doi.org/10.1016/j.earscirev.2016.02.002>
- 523 Vacchi, M., Ghilardi, M., Spada, G., Currás, A., Robresco, S., 2017. New insights
524 into the sea-level evolution in Corsica (NW Mediterranean) since the late
525 Neolithic. *Journal of Archaeological Science: Reports* 12, 782–793.
526 <https://doi.org/10.1016/j.jasrep.2016.07.006>
- 527 Vacchi, M., Ghilardi, M., Melis, R. T., Spada, G., Giaime, M., Marriner, N.,
528 Lorscheid, T., Morhange, C., Burjachs, F., Rovere, A., 2018. New relative sea-
529 level insights into the isostatic history of the Western Mediterranean. *Quaternary*
530 *Science Reviews* 201, 396–408.
531 <https://doi.org/10.1016/J.QUASCIREV.2018.10.025>
- 532 Vamvakaris, D.A., Papazachos, C.B., Papaioannou, C.A., Scordilis, E.M., Karakaisis,
533 G.F., 2016. A detailed seismic zonation model for shallow earthquakes in the
534 broader Aegean area. *Natural Hazards and Earth System Sciences* 16, 55–84.
535 doi:10.5194/nhess-16-55-2016
- 536 Van De Plassche, O., Wright, A. J., Horton, B. P., Engelhart, S. E., Kemp, A. C.,
537 Mallinson, D., Kopp, R. E., 2014. Estimating tectonic uplift of the Cape Fear Arch
538 (south-eastern United States) using reconstructions of Holocene relative sea level.
539 *Journal of Quaternary Science* 29(8), 749–759. <https://doi.org/10.1002/jqs.2746>
- 540 Woodroffe, S. A., Long, A. J., Milne, G. A., Bryant, C. L., Thomas, A. L., 2015. New
541 constraints on late Holocene eustatic sea-level changes from Mahé, Seychelles.

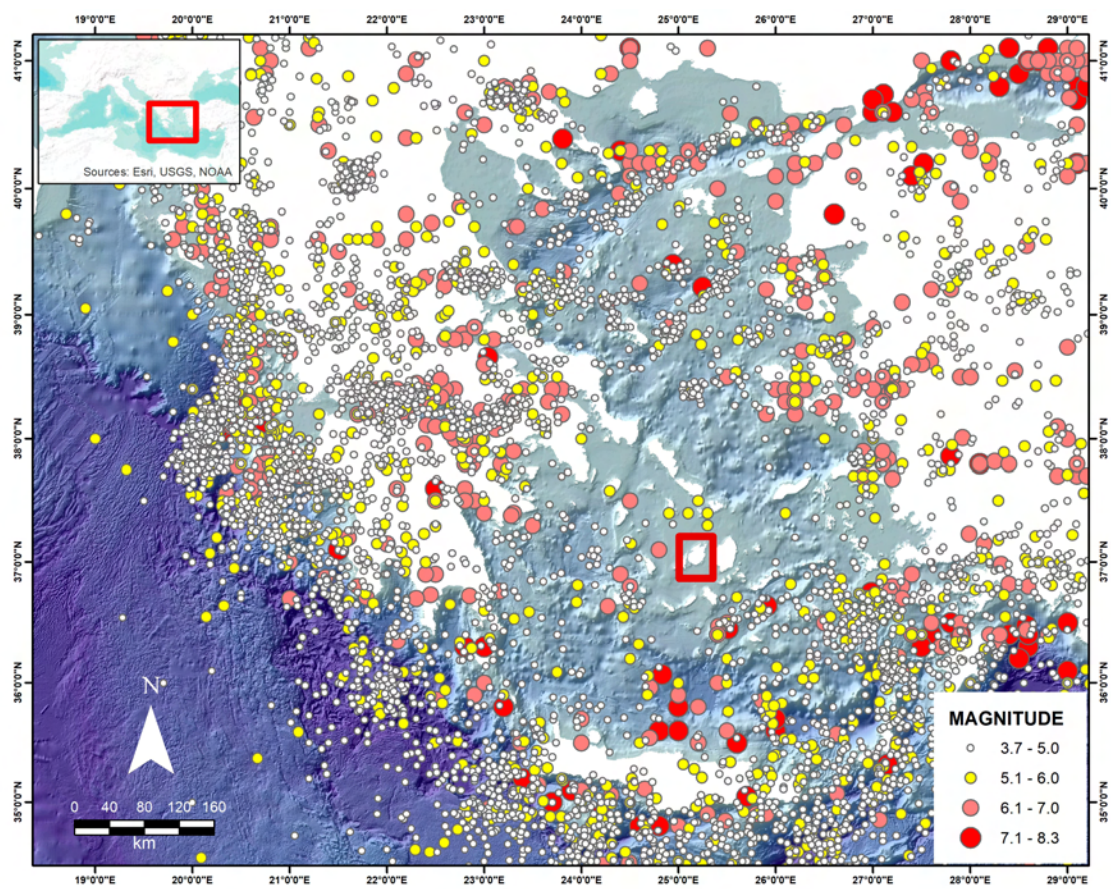
542 Quaternary Science Reviews, 115, 1–16.

543 <https://doi.org/10.1016/J.QUASCIREV.2015.02.011>

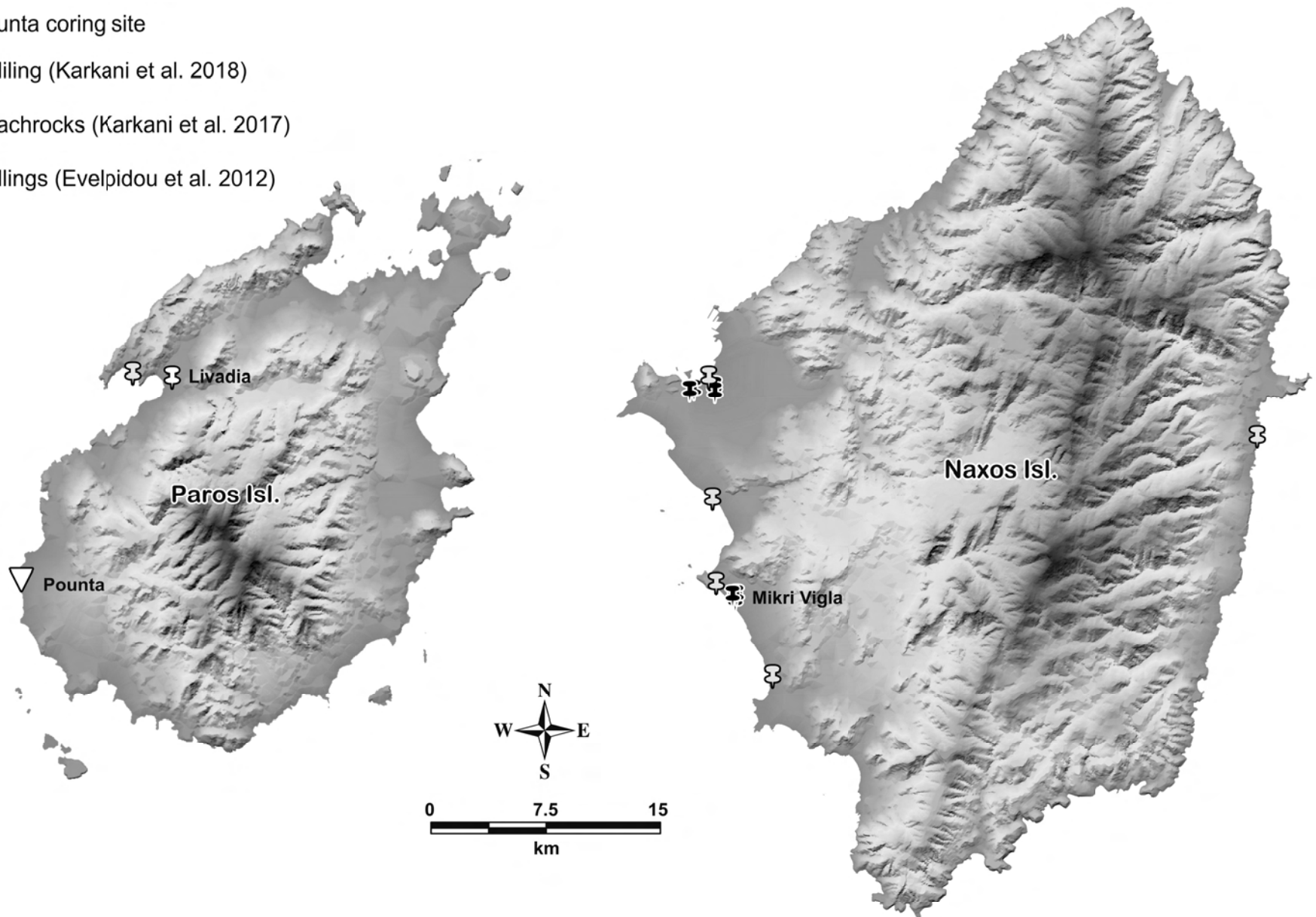
ACCEPTED MANUSCRIPT

Table 1. Radiocarbon ages for dated samples from the Paros core. The data were calibrated using the online software Calib 7.10 (Stuiver et al., 2016) with the Marine13 curve (Reimer et al., 2013). Shell samples were corrected for the local marine reservoir effect according to Reimer & McCormac (2002), using a mean ΔR value of 154 ± 52 for the Aegean Sea.

Sample code	Lab code	Depth below sea level (m)	Material	$\delta^{13}\text{C}$	^{14}C BP	Age cal. BP	Cal. BC/AD (2σ)
POU2-1	Poz-81147	85	Conus mediterraneus	2.8	520 \pm 30	-	-
POU2-2	Poz-81148	186-196	Loripes lacteus	0.3	715 \pm 30	40-298	1652-1910 AD
POU2-3	Poz-81354	260-270	Cerithium vulgatum	-3.9	1475 \pm 30	721-986	964-1229 AD
POU2-4	Poz-81140	337-346	Nassarius lousi	4.9	490 \pm 30	-	-

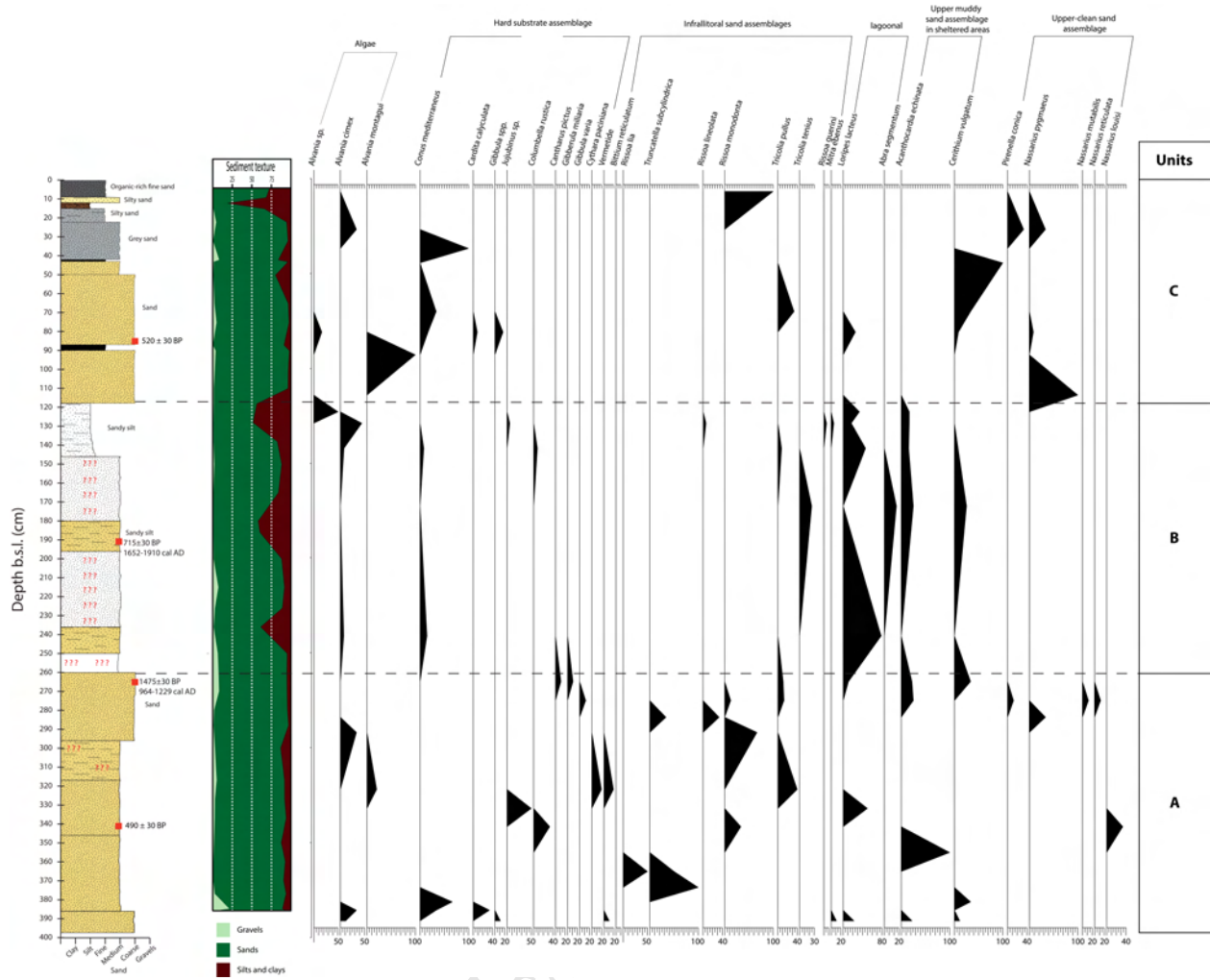


- ▽ Pounta coring site
- ⊗ Drilling (Karkani et al. 2018)
- ⊗ Beachrocks (Karkani et al. 2017)
- ⊗ Drillings (Evelpidou et al. 2012)

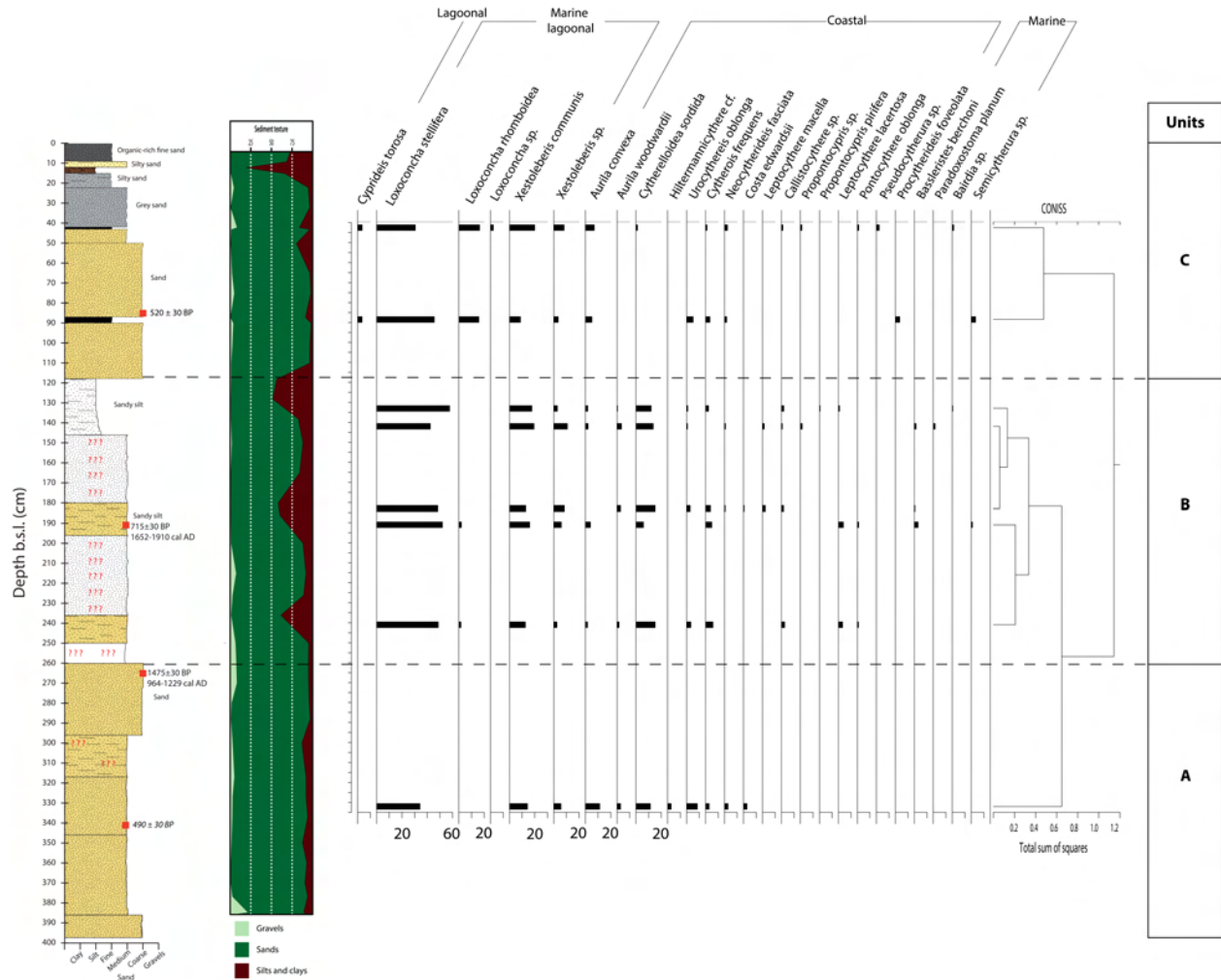




MANUSCRIPT



ACCEPTED



ACCEPTED

